Giant Magnetodrag in Graphene at Charge Neutrality

M. Titov,[1] R. V. Gorbachev,[2,3] B. N. Narozhny,[4] T. Tudorovskiy,[1] M. Schütt,[5] P. M. Ostrovsky,[6,5,7] I. V. Gornyi,[5,8]
A. D. Mirlin,[5,4,9] M. I. Katsnelson,[1] K. S. Novoselov,[2] A. K. Geim,[2,3] and L. A. Ponomarenko[2]

[1]*Radboud University Nijmegen, Institute for Molecules and Materials, NL-6525 AJ Nijmegen, Netherlands*
[2]*School of Physics and Astronomy, University of Manchester, Manchester M13 9PL, United Kingdom*
[3]*Centre for Mesoscience and Nanotechnology, University of Manchester, Manchester M13 9PL, United Kingdom*
[4]*Institut für Theorie der Kondensierten Materie and DFG Center for Functional Nanostructures,*
Karlsruhe Institute of Technology, 76128 Karlsruhe, Germany
[5]*Institut für Nanotechnologie, Karlsruhe Institute of Technology, 76021 Karlsruhe, Germany*
[6]*Max-Planck-Institut für Festkörperforschung, Heisenbergstrasse 1, 70569, Stuttgart, Germany*
[7]*L. D. Landau Institute for Theoretical Physics RAS, 119334 Moscow, Russia*
[8]*A.F. Ioffe Physico-Technical Institute, 194021 St. Petersburg, Russia*
[9]*Petersburg Nuclear Physics Institute, 188350 St. Petersburg, Russia*
(Received 1 April 2013; published 14 October 2013)

We report experimental data and theoretical analysis of Coulomb drag between two closely positioned graphene monolayers in a weak magnetic field. Close enough to the neutrality point, the coexistence of electrons and holes in each layer leads to a dramatic increase of the drag resistivity. Away from charge neutrality, we observe nonzero Hall drag. The observed phenomena are explained by decoupling of electric and quasiparticle currents which are orthogonal at charge neutrality. The sign of magnetodrag depends on the energy relaxation rate and geometry of the sample.

Recent measurements [1] of frictional drag in graphene-based double-layer devices revealed the unexpected phenomenon of giant magnetodrag at charge neutrality. Applying external magnetic fields as weak as 0.1–0.3 T results in a reversal of the sign and a dramatic enhancement of the amplitude of the drag resistance. If the device is doped away from charge neutrality, the impact of such a weak field on the drag resistance is very modest. The observed effect weakens at low temperatures, hinting at the classical origin of the phenomenon.

In this Letter, we report experimental data on longitudinal and Hall drag resistivity in isolated graphene layers separated by a 1 nm thick boron-nitride (hBN) spacer. The observed effects are explained in terms of coexisting electron and hole liquids in each layer [2,3]. This theory is based on the hydrodynamic description of transport in graphene derived in Refs. [4–6] using the quantum kinetic equation (QKE) framework [7,8]. It provides a simplified description of magnetodrag while capturing the essentially classical physics of the phenomenon [9]. The effect can be traced back to the fact that the Lorentz force in the electron and hole bands has the opposite sign, which is also the reason for the anomalously large Nernst effect [10,11] and vanishing Hall effect at charge neutrality.

The classical mechanism behind giant magnetodrag is illustrated in Fig. 1. The upper panel shows two infinite graphene layers at charge neutrality. The driving electric current j_1 in the active layer corresponds to the counter-propagating flow of electrons and holes with zero total momentum due to exact electron-hole symmetry (hence, in the absence of additional correlations there is no drag at

the Dirac point [5,12–15]). In a weak magnetic field, electrons and holes are deflected by the Lorentz force and drift in the same direction. The resulting quasiparticle flow P_1 carries nonzero momentum in the direction
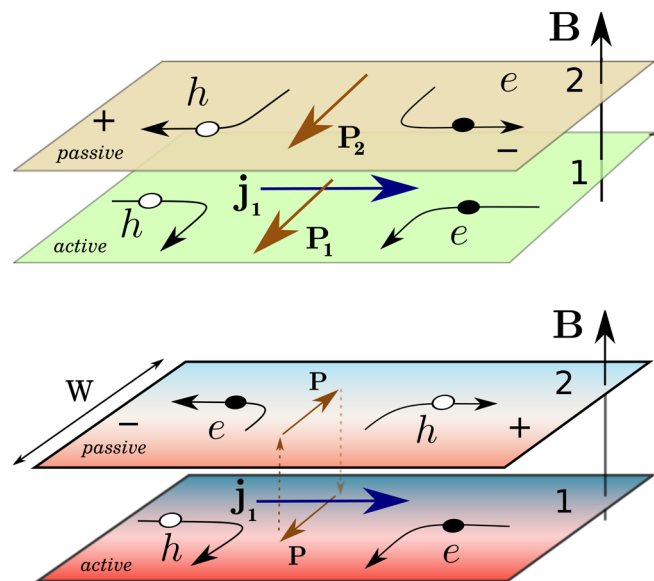

FIG. 1 (color online). Mechanism of magnetodrag at charge neutrality. Upper panel: In an infinite system quasiparticle currents P_i in the two layers flow in the same direction, leading to positive drag $\rho_{xx}^D = V_2/j_1 > 0$. Lower panel: In a thermally isolated system no net quasiparticle flow is possible (leading to inhomogeneities in the quasiparticle density); quasiparticle currents in the two layers have opposite directions yielding negative drag.

perpendicular to j_1. Momentum transfer by the interlayer Coulomb interaction induces the quasiparticle current P_2 in the same direction as P_1. Lorentz forces acting on both types of carriers in the passive layer drive the charge flow in the direction opposite to j_1. In an open circuit, this current is compensated by a finite voltage V_2, yielding a positive drag resistivity $\rho_{xx}^D = V_2/j_1 > 0$.

This mechanism of magnetodrag is closely related to the anomalous Nernst effect in single-layer graphene [4,10,11]. At charge neutrality, the quasiparticle current is proportional to the heat current. A similar mechanism, where the role of P_i is played by spin currents, has been proposed in Ref. [16] as a possible explanation for a giant nonlocal magnetoresistance.

The above argument describes the steady state in infinite systems where all physical quantities are homogeneous in real space. This is not the case in relatively small, mesoscopic samples. Whether a particular sample should be considered "small" or "large" is determined by comparing the sample size to the typical length scale of the leading relaxation process. At high enough temperatures, energy is most efficiently relaxed by electron-phonon scattering, which we describe in this Letter by the length ℓ_{ph} [17,18].

In a finite system, quasiparticle currents must vanish at the boundaries. For $W \gg \ell_{\text{ph}}$, the quasiparticle current and density is homogeneous in the bulk and the system remains effectively infinite.

For $W \ll \ell_{\text{ph}}$, the currents P_i become y dependent. In this case, energy conservation dictates $P_2(y) = -P_1(y)$. As a result, electric charge in the passive layer tends to flow in the same direction as j_1 (see Fig. 1), yielding negative drag (similarly to Coulomb drag in single-band systems).

In order to test the above ideas, we perform new measurements of the drag effect in a magnetic field, illustrated in Fig. 2. The experiments [19] are carried out on a graphene double-layer structure with a 1 nm hBN spacer and two electrostatic gates. Despite the small thickness of the spacer, the tunneling resistance between the layers >300 kΩ gives only a negligible leakage contribution to the drag <0.5 Ω [19,20]. The schematics of the experiment are shown in the inset of Fig. 2(e). The same device was used in Ref. [1] for drag measurements in zero magnetic field.

The map for the drag resistivity, $\rho_{xx}^D(V_T, V_B)$, is shown in Fig. 2(a) at $T = 240$ K. The main difference compared to the zero field experiment reported earlier [1] is large
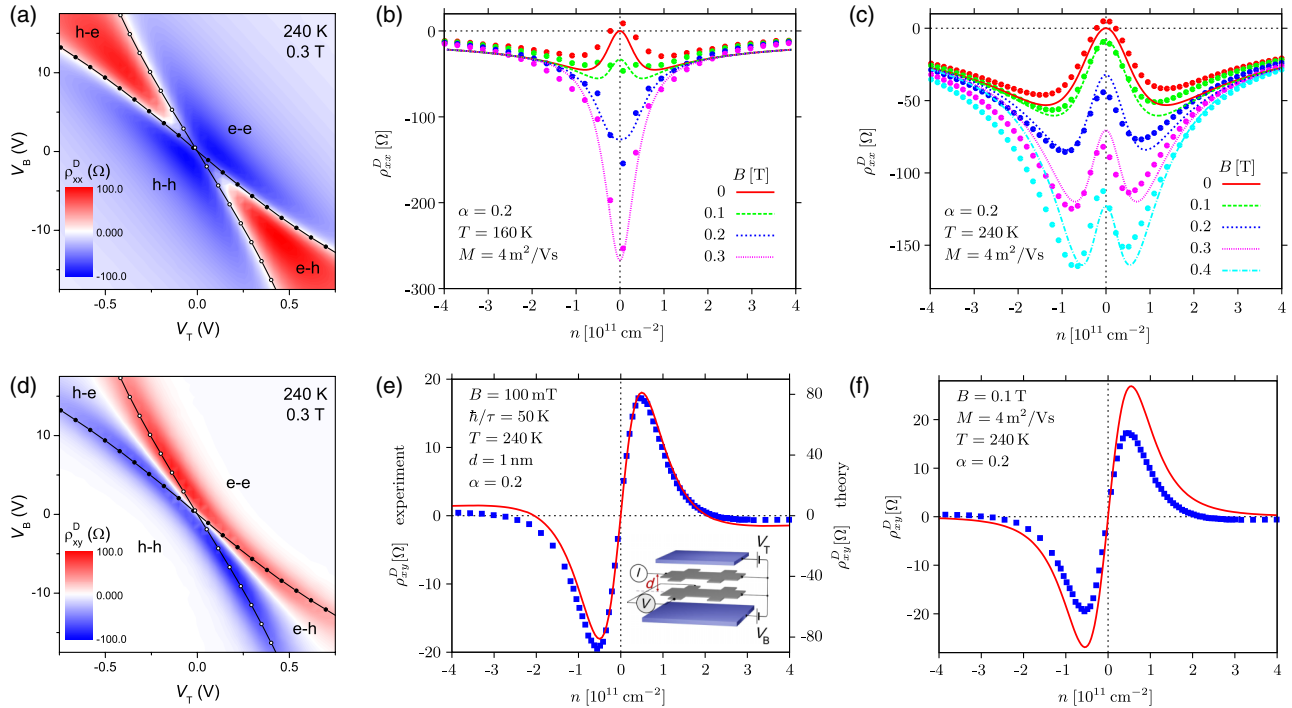

FIG. 2 (color online).   (a) Longitudinal drag resistivity in magnetic field as a function of the top (V_T) and bottom (V_B) gate voltages. Lines track positions of maxima in single-layer resistivity in top (open symbols) and bottom (solid symbols) layers. (b) Magnetodrag for $n_1 = n_2 = n$ at $T = 160$ K. Solid symbols represent the experimental data. The error bars for the data are within the symbol size. The theoretical lines show solutions to Eqs. (6). (c) Magnetodrag for $n_1 = n_2 = n$ at $T = 240$ K. Solid symbols: experimental data; lines: theory (6). (d) Map of Hall drag resistivity as a function of V_T and V_B. The white diagonal area corresponds to vanishing Hall drag for $n_1 = -n_2$. The lines are the same as in (a). (e) Experimental data (blue squares, left axis) and theory (red solid line, right axis) for the Hall drag resistivity for $n_1 = n_2 = n$. The theoretical curve is calculated on the basis of the microscopic theory of Ref. [5]. Note the sign change at $n \approx \pm 2 \times 10^{11}$ cm^{-2}. Inset: schematics of Hall drag measurements in double-layer system. (f) Hall drag resistivity for $n_1 = n_2 = n$. The data (blue squares) are identical to those in (e); the red solid line represents solutions to Eq. (6).

negative drag at the double neutrality point. A dramatic change in drag resistivity with the applied magnetic field is shown in more detail in Figs. 2(b) and 2(c) (at 160 and 240 K, respectively). To ensure the same charge densities n_1 and n_2 in the top and bottom layers, we sweep both gates simultaneously along the line connecting the bottom left and top right corners of the map. The experiment shows a large negative drag resistivity close to the double neutrality point, $n_1 = n_2 = 0$, as expected for a small sample (see above); in our device both layers have the width $W \approx 2\ \mu$m and sufficiently resistive contacts.

In addition to the longitudinal drag resistivity we also measure the Hall drag resistivity, $\rho_{xy}^D(V_T, V_B)$, shown in Fig. 2(d) at $T = 240$ K as a function of the top and bottom gate voltages. Because of the low density of states in graphene and the small separation between layers ($d \approx 1$ nm, interlayer capacitance $\sim 2.2\ \mu$F/cm^2), the relationship between gate voltages and charge densities is rather nontrivial (see the Supplemental Material [19]). To identify signs of charge carriers at each point in Fig. 2(d), we also measured resistivity maps for both layers. Since the resistance of graphene is peaked at charge neutrality, tracking the position of the resistivity maximum gives the lines which divide the map into the electron- and hole-doped parts. Such lines are shown in both maps; see Figs. 2(a) and 2(d). The observed Hall drag resistance is large when one of the layers is close to the neutrality point and vanishes if two layers have the same charge densities with opposite signs (a white line running from the top left to bottom right corner).

We now turn to the theoretical description of the drag effect. Consider first the Drude model for electrons and holes in two layers,

$$e\boldsymbol{E}_i + e[\boldsymbol{v}_{ie} \times \boldsymbol{B}] = \boldsymbol{F}_{ie} + e\boldsymbol{v}_{ie}/M_i, \qquad (1a)$$

$$-e\boldsymbol{E}_i - e[\boldsymbol{v}_{ih} \times \boldsymbol{B}] = \boldsymbol{F}_{ih} + e\boldsymbol{v}_{ih}/M_i, \qquad (1b)$$

where $i = 1, 2$, $a = e, h$, $\boldsymbol{v}_{ia}$ stand for the mean velocities of electrons and holes in the layer i, $\boldsymbol{E}_i$ and $\boldsymbol{B}$ are electric and magnetic fields, and M_i are the carrier mobilities due to impurity scattering. The electric $\boldsymbol{j}_i$ and quasiparticle $\boldsymbol{P}_i$ currents are related to $\boldsymbol{v}_{ia}$ by [2]

$$\boldsymbol{j}_i = e(n_{ie}\boldsymbol{v}_{ie} - n_{ih}\boldsymbol{v}_{ih}), \qquad \boldsymbol{P}_i = n_{ie}\boldsymbol{v}_{ie} + n_{ih}\boldsymbol{v}_{ih}, \qquad (2)$$

with $n_{ie(h)} = \int_0^\infty d\varepsilon \nu(\varepsilon)[e^{(\varepsilon \mp \mu_i)/T} + 1]^{-1}$ standing for the electron and hole densities, $\nu(\varepsilon) = 2|\varepsilon|/\pi(\hbar v)^2$ being the density of states in graphene at $B = 0$, and μ_i are the chemical potentials measured from the Dirac point. The total charge and quasiparticle densities are defined as $n_i = n_{ie} - n_{ih}$ and $\rho_i = n_{ie} + n_{ih}$.

The frictional force acting on each type of carrier can be represented as

$$\boldsymbol{F}_{ia} = \hbar \sum_{jb} [\gamma_{ij}^{ab} n_{jb}(\boldsymbol{v}_{ia} - \boldsymbol{v}_{jb}) + \tilde{\gamma}_{ij}^{ab} n_{jb}(\boldsymbol{v}_{ia} + \boldsymbol{v}_{jb})], \qquad (3)$$

where the coefficients $\tilde{\gamma}$ appear in monolayer graphene due to the absence of Galilean invariance. The expression (3) can be obtained by solving the QKE in the hydrodynamic approximation [4–7,21].

For $n_i = 0$, the first term in Eq. (3) simplifies to

$$\boldsymbol{F}_{1a} = -\boldsymbol{F}_{2a} = \boldsymbol{F} = \hbar\gamma(\boldsymbol{P}_1 - \boldsymbol{P}_2), \qquad (4)$$

where $\gamma = \hbar/(T\tau_P)$, with τ_P^{-1} being the momentum relaxation rate. The second term in Eq. (3) renormalizes the mobilities [5,7,8]. The Drude model (1) with the force (4) also describes the case $\mu_i \gg T$, where $\gamma = \hbar/(\mu\tau_P)$. In both limits, the model (1) is equivalent to the hydrodynamic transport equations derived from the QKE [5,21].

For strongly doped graphene, $\mu_i \gg T$, the quasiparticle current and density are obsolete: $\boldsymbol{P}_i = \boldsymbol{j}_i/e$ and $\rho_i = n_i$. Equations (1) are then reduced to the standard Drude model yielding conventional drag $\rho_{xx}^D = E_{2x}/j_{1x} = -\hbar\gamma/e^2$ with negligible dependence on the magnetic field [22] and vanishing Hall drag $\rho_{xy}^D = E_{2y}/j_{1x} = 0$.

In contrast, at charge neutrality the quasiparticle and charge degrees of freedom are inequivalent. The quasiparticle density for $n_i = 0$ is determined by the temperature, $\rho_i = \rho_0 = \pi T^2/3(\hbar v)^2$, while the currents $\boldsymbol{j}_1$ and $\boldsymbol{P}_i$ become orthogonal; see Fig. 1.

Rewriting Eqs. (1) and (4) in terms of currents, we obtain the resistivity tensor. For $n_i = 0$, the longitudinal drag resistivity is given by

$$\rho_{xx}^D(n_i = 0) = \frac{\hbar\gamma}{e^2} \frac{B^2 M_1 M_2}{1 + \hbar\gamma\rho_0(M_1 + M_2)/e}, \qquad (5)$$

which describes positive drag in an infinite system in agreement with the qualitative picture; see Fig. 1, upper panel. In the limit of weak interaction, $\gamma M T^2 \ll \hbar e v^2$, the result (5) can be obtained from the standard perturbative approach [13] modified for graphene in the classical magnetic field.

The large negative peak in ρ_{xx}^D at the double neutrality point [Fig. 2(b)] suggests that the sample width $W \approx 2\ \mu$m is relatively small as compared to ℓ_{ph} (Fig. 1, lower panel). To account for the finite sample width, we rewrite the equations (1) in terms of the currents $\boldsymbol{j}_i$ and $\boldsymbol{P}_i$ and allow for the spatially varying quasiparticle density, $\rho_i(y)$. The resulting model for the first layer reads

$$-K_1\boldsymbol{\nabla}\rho_1 + en_1\boldsymbol{E}_1 + [\boldsymbol{j}_1 \times \boldsymbol{B}] = \rho_1\boldsymbol{F} + e\boldsymbol{P}_1/M_1, \qquad (6a)$$

$$e\rho_1\boldsymbol{E}_1 + e[\boldsymbol{P}_1 \times \boldsymbol{B}] = n_1\boldsymbol{F} + \boldsymbol{j}_1/M_1, \qquad (6b)$$

$$\boldsymbol{\nabla} \cdot \boldsymbol{P}_1 = -(\rho_1 - \rho_0)/\tau_{ph} - (\rho_1 - \rho_2)/(2\tau_Q). \qquad (6c)$$

Here $K_i = (\pi\hbar^2 v^2/2)(\partial n_i/\partial \mu_i) = 2T\ln(2\cosh\mu_i/2T)$ is the mean quasiparticle kinetic energy. In the second layer the force $\boldsymbol{F}$ enters with the opposite sign. The continuity equation for the quasiparticle current [Eq. (6c)] includes relaxation by the electron-hole recombination [2], with $\tau_{\rm ph}^{-1}$ describing the energy loss from the system, which is dominated by phonon scattering (see the Supplemental Material [19]); τ_Q^{-1} characterizes quasiparticle imbalance relaxation due to interlayer Coulomb interaction. For $\tau_{\rm ph}^{-1} = 0$, the hard-wall boundary conditions in y directions require $\boldsymbol{P}_1 + \boldsymbol{P}_2 = 0$. Near the Dirac point, energy and momentum relaxation rates coincide ($\tau_Q \sim \tau_P$). In doped graphene, recombination rates are exponentially suppressed [19].

The continuity equation for the electric current simply reads $\boldsymbol{\nabla} \cdot \boldsymbol{j}_i = 0$; hence, $\boldsymbol{j}_i = (j_i(y), 0)$. Within linear response, the equilibrium density ρ_0 has to be substituted into products $\rho_i\boldsymbol{F}$ and $\rho_i\boldsymbol{E}$. This way we obtain the linear system of differential equations for $P_{iy}(y)$, $j_{1x}(y)$, and $\rho_i(y)$. Since the charge current acquires the dependence y coordinate, we define $\rho_{xx}^D = E_{2x}/\langle j_{1x}\rangle$, where $\langle j_{1x}\rangle = W^{-1}\int_0^W j_{1x}dy$.

The model (6) with the frictional force (4) admits a full analytic solution (see the Supplemental Material [19]) in terms of τ_Q^{-1}, $\tau_{\rm ph}^{-1}$, and τ_P^{-1}. The resulting behavior crucially depends on these rates: in particular, in the absence of phonons ($\tau_{\rm ph} \to \infty$, i.e., in a thermally isolated system) drag at the Dirac point is always negative; see Fig. 1. For vanishing sample width ($W \to 0$), we find $\rho_{xx}^D \approx -B^2W^2/(24\rho_0 K\tau_Q)$. In general, these rates depend on n_i and have to be determined by the microscopic theory [5]. Relegating further mathematical details to the Supplemental Material [19], we present the results of our calculations in Fig. 2 alongside experimental data.

The drag resistivity ρ_{xx}^D is plotted in Figs. 2(b) and 2(c) for $T = 160$ K and $T = 240$ K, respectively. The exponential collapse of theoretical curves at high carrier density is an artifact of our phenomenological model [17,19]. At higher temperature [Fig. 2(c)], the drag resistivity exhibits qualitatively new features near charge neutrality which can be physically attributed to higher efficiency of relaxation processes. The sign of ρ_{xx}^D at the Dirac point is then determined by the relation between the typical relaxation length $\ell_{\rm ph} = 2\sqrt{K\tau_{\rm ph}M/e}$ and the sample width. This is illustrated in Fig. 3, where we plot ρ_{xx}^D as a function of magnetic field for different values of W choosing realistic values for $T = 240$ K, $M = 4$ m^2/Vs, and $\ell_{\rm ph} = 1.2$ μm.

Based on the above results, we predict that in wider samples giant magnetodrag at the Dirac point should become positive. We also speculate that magnetodrag at charge neutrality may become positive in stronger fields due to the magnetic-field dependence of the scattering times τ_Q, τ_P, and $\tau_{\rm ph}$.

The model (6) allows us to calculate the Hall drag resistivity ρ_{xy}^D. The result is shown in Fig. 2(f). The theory
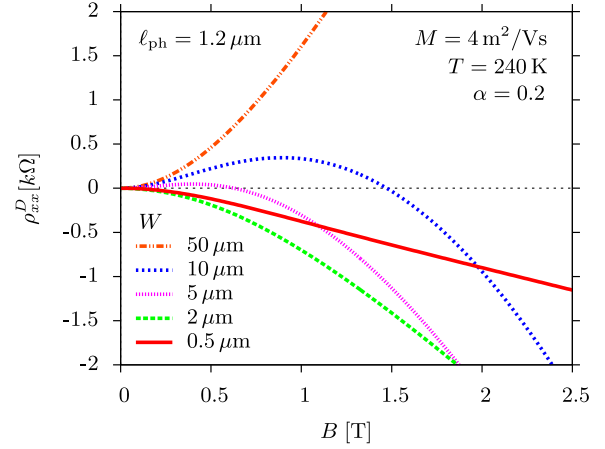

FIG. 3 (color online). The magnetic field dependence of the longitudinal drag resistivity at the neutrality point. The positive sign of the magnetodrag in weak fields corresponds to the limit $W \gg \ell_{\rm ph}$, where $\ell_{\rm ph} \approx 1.2$ μm for the parameters of the plot. The magnetic-field dependence of scattering rates is disregarded in the plot.

also predicts vanishing Hall drag for the case of oppositely doped layers, $n_1 = -n_2$. Interestingly enough, the data show a sign change of ρ_{xy}^D at $n \approx \pm 2 \times 10^{11}$ cm^{-2}. At that point the effect is rather weak and requires a more accurate consideration. Using the microscopic theory of Ref. [5], we have evaluated the Hall drag resistivity for an infinite sample with an energy-independent impurity scattering time τ. The value of τ was determined from the measured single-layer resistivity and we have used the most plausible estimate for the effective electron-electron interaction parameter in graphene on hBN, $\alpha \approx 0.2$. The result is shown in Fig. 2(e) along with the corresponding experimental data without any fitting.

In conclusion, we have measured the longitudinal and Hall drag resistivity in double-layer graphene and provided a theoretical description of the observed effects. Giant magnetodrag at the neutrality point appears due to the presence of two types of carriers (electrons and holes), which in weak magnetic fields experience a unidirectional drift orthogonal to the driving current. This effect is specific to the neutrality point, where nonzero drag appears despite the exact electron-hole symmetry. Our theory does not rely on the Dirac spectrum in graphene, but is equivalent to the microscopic theory [5,9] at and far away from charge neutrality, capturing the essential physics of magnetodrag. For a more accurate description of the effect at intermediate densities, the microscopic theory should be formulated on the basis of the QKE [21].

Note added.—Recently, we became aware of a related work by Song and Levitov [23].

---

[1] R. V. Gorbachev, A. K. Geim, M. I. Katsnelson, K. S. Novoselov, T. Tudorovskiy, I. V. Grigorieva, A. H. MacDonald, K. Watanabe, T. Taniguchi, and L. A. Ponomarenko, Nat. Phys. **8,** 896 (2012).

[2] M. S. Foster and I. L. Aleiner, Phys. Rev. B **79,** 085415 (2009).

[3] D. Svintsov, V. Vyurkov, S. Yurchenko, T. Otsuji, and V. Ryzhii, J. Appl. Phys. **111,** 083715 (2012).

[4] M. Müller and S. Sachdev, Phys. Rev. B **78,** 115419 (2008); M. Müller, L. Fritz, and S. Sachdev, *ibid.* **78,** 115406 (2008).

[5] M. Schütt, P. M. Ostrovsky, M. Titov, I. V. Gornyi, B. N. Narozhny, and A. D. Mirlin, Phys. Rev. Lett. **110,** 026601 (2013); M. Schütt, Ph.D. thesis, Karlsruhe Institute of Technology (KIT), 2013, http://digbib.ubka.uni-karlsruhe.de/volltexte/1000036515.

[6] J. Lux and L. Fritz, Phys. Rev. B **86,** 165446 (2012).

[7] L. Fritz, J. Schmalian, M. Müller, and S. Sachdev, Phys. Rev. B **78,** 085416 (2008); M. Müller, J. Schmalian, and L. Fritz, Phys. Rev. Lett. **103,** 025301 (2009).

[8] A. B. Kashuba, Phys. Rev. B **78,** 085415 (2008).

[9] The hydrodynamic description of drag in graphene derived in Ref. [5] was justified by the singular behavior of the collision integral due to kinematics of Dirac fermions. This singularity leads to the fast unidirectional thermalization and allows one to select the relevant eigenmodes of the collision integral [4,7]. Projecting the collision integral onto these modes, one arrives at the effective model, which is equivalent to Eq. (1) with the generalized force (4).

[10] Y. M. Zuev, W. Chang, and P. Kim, Phys. Rev. Lett. **102,** 096807 (2009).

[11] P. Wei, W. Z. Bao, Y. Pu, C. N. Lau, and J. Shi, Phys. Rev. Lett. **102,** 166808 (2009).

[12] W. K. Tse, Ben Yu-Kuang Hu, and S. Das Sarma, Phys. Rev. B **76,** 081401 (2007).

[13] B. N. Narozhny, M. Titov, I. V. Gornyi, and P. M. Ostrovsky, Phys. Rev. B **85,** 195421 (2012).

[14] M. Carrega, T. Tudorovskiy, A. Principi, M. I. Katsnelson, and M. Polini, New J. Phys. **14,** 063033 (2012).

[15] B. Amorim and N. M. R. Peres, J. Phys. Condens. Matter **24,** 335602 (2012).

[16] D. A. Abanin, S. V. Morozov, L. A. Ponomarenko, R. V. Gorbachev, A. S. Mayorov, M. I. Katsnelson, K. Watanabe, T. Taniguchi, K. S. Novoselov, L. S. Levitov, and A. K. Geim, Science **332,** 328 (2011).

[17] The microscopic theory [5,21] includes thermoelectric effects formulated in terms of energy currents. The corresponding hydrodynamic description yields only the power-law decay of the magnetodrag at $\mu_i \gg T$, in contrast to the exponential collapse shown in Figs. 2(b) and 2(c). At the Dirac point the energy current is equivalent to the quasiparticle current $\boldsymbol{P}$.

[18] J. C. W. Song, M. Y. Reizer, and L. S. Levitov, Phys. Rev. Lett. **109,** 106602 (2012).

[19] See Supplemental Material at http://link.aps.org/supplemental/10.1103/PhysRevLett.111.166601 for details.

[20] Y. Oreg and B. I. Halperin, Phys. Rev. B **60,** 5679 (1999).

[21] M. Schütt *et al.* (to be published).

[22] A.-P. Jauho and H. Smith, Phys. Rev. B **47,** 4420 (1993); K. Flensberg, Ben Yu-Kuang Hu, A.-P. Jauho, and J. M. Kinaret, Phys. Rev. B **52,** 14 761 (1995); A. Kamenev and Y. Oreg, Phys. Rev. B **52,** 7516 (1995).

[23] J. C. W. Song and L. S. Levitov, Phys. Rev. Lett. **111,** 126601 (2013).